

In-flight stability of quantum cascade laser-based infrared absorption spectroscopy measurements of atmospheric carbon monoxide

Ivan Tadic¹  · Uwe Parchatka¹ · Rainer Königstedt¹ · Horst Fischer¹

Received: 31 January 2017 / Accepted: 3 April 2017 / Published online: 18 April 2017
© The Author(s) 2017. This article is an open access publication

Abstract Airborne carbon monoxide (CO) measurements based on Quantum cascade Laser infrared Absorption Spectroscopy (QLAS) were performed on the German High-Altitude Long-range Observatory (HALO) aircraft during test flights in January 2015. Here we investigate the in-flight stability of TRISTAR (TRacer In-Situ Tdlas for Atmospheric Research), a multilaser QLAS instrument for the detection of tropospheric CO, methane and formaldehyde (HCHO). During one test flight the instrument was probed with tank air to measure a constant mixing ratio of CO and zero air for HCHO. Here we investigate the instrument stability for the CO channel of TRISTAR and identify potential noise sources as well as environmental processes that limit the stability of the instrument. The 1σ reproducibility of the constant CO measurement yields a value of 1.2% (2.9 ppb_v) corresponding to an optical density limit of 0.001 for a 5-s average. The CO precision is ultimately limited by an etalon fringe originating from the double corner-cube White cell, whose phase and amplitude changes with the aircraft heading.

1 Introduction

Mid infra-red absorption spectroscopy is a versatile tool to quantify mixing ratios of atmospheric trace gases at ppb_v

and sub-ppb_v levels. In particular, the use of tunable infrared lasers has found widespread application during the past four decades. While instruments in the 1980s and 1990s deployed lead-chalcogenide tunable diode lasers [1–4], since about the year 2000 tunable quantum cascade lasers have mostly been used due to their superior behavior with respect to laser power, single mode operation and stability [5–7]. In particular, the deployment of Tunable Diode Laser Absorption Spectroscopy (TDLAS) or Quantum cascade Laser Absorption Spectroscopy (QLAS) instruments on research aircraft require compact, low weight and rigid designs to face the challenging demands due to vibrations, as well as cabin pressure and temperature fluctuations on the platform [5, 6, 8–12]. Since 1997, we have deployed the multi-laser TRacer In-Situ Tdlas for Atmospheric Research (TRISTAR) on a number of airborne platforms during a total of 15 measurement campaigns, on 170 research flights with more than 800 flight hours for tropospheric and stratospheric measurements of carbon monoxide (CO), carbon dioxide (CO₂), methane (CH₄), nitrous oxide (N₂O) and formaldehyde (HCHO) [13, 14]. In the present configuration TRISTAR deploys three liquid nitrogen cooled continuous wave quantum cascade lasers for CO, CH₄ and HCHO. As mentioned above, the measurement precision during airborne applications suffers from a non-ideal environment. In particular, changes of the cabin temperature and the cabin pressure can affect the optical alignment and the operation conditions of lasers and infra-red detectors. For species with mixing ratios in the ppb_v to ppm_v range like CO (typical tropospheric mixing ratios of 80 ppb_v) and CH₄ (~2 ppm_v) the absorptions correspond to optical densities in the 10⁻² range and the reported in-flight precisions, based on the reproducibility of in-flight calibrations, are in the sub per cent range [14], similar to results obtained with other airborne QCL spectrometers [15, 16]. For HCHO, whose tropospheric mixing

This article is part of the topical collection “Field Laser Applications in Industry and Research” guest edited by Francesco D’Amato, Erik Kerstel, and Alan Fried.

✉ Ivan Tadic
i.tadic@mpic.de

¹ Max Planck Institute for Chemistry, Hahn-Meitner-Weg 1, 55128 Mainz, Germany

ratio is in the sub-ppbv range, corresponding to optical densities of the order of 10^{-5} , the detection limit is more important than instrument precision. Reported values based on the reproducibility of zero air measurements are in the low tens of ppt_v range and are limited by optical fringes [14]. In order to improve both the precision of CO and CH₄ measurements and the detection limit for HCHO, the instrument has to be stabilized with respect to the changing environmental processes, such as pressure, temperature and aircraft movements and vibrations. This requires a detailed knowledge of the parameters affecting the instrument stability during airborne operations. In January 2015 TRISTAR together with other trace gas instruments was installed onboard the German High-Altitude Long-range Observatory (HALO) aircraft for the Oxidation Mechanism Observations (OMO) project. Since the payload was new, a number of test flights were performed during the first phase of OMO-Europe (OMO-EU). During one of these flights we had a chance to test the in-flight instrument stability under controlled conditions. For this purpose TRISTAR was operated in a dual channel mode (CO and HCHO), sampling either a CO standard from a tank or zero air from scrubbing HCHO from the same tank. Since the CO and HCHO measurements were made with a constant signal input, the in-flight data provide insight into the instrument stability under changing environment conditions such as temperature, pressure and position changes due to flight level changes and aircraft heading. Here we will discuss results for the CO measurements. Results for HCHO will be addressed in a separate study. Please note that TRISTAR was autonomous in operation. Although 4 operators were supervising the instruments operated on HALO (15 instruments in total), no trained operator was dedicated to the operation of TRISTAR.

The paper is structured as follows: Sect. 2 provides a short description of TRISTAR. Since the main features of the instrument have been discussed in a number of previous publications [13, 14, 17], we will mainly address recent changes and specific conditions for the operation on HALO. The results from the in-flight stability tests will be presented in Sect. 3, while in Sect. 4 applications of ambient CO data obtained during two measurement flights will be discussed to illustrate the data quality. Finally (Sect. 5), we will summarize the obtained results and give an outlook for future instrument improvements.

2 Instrument set-up

TRISTAR is a robust and compact 3-laser spectrometer that was developed in 1997 for airborne trace gas measurements. In the HALO configuration the optical board is mounted on top of a 19" half rack. The instruments electronics (laser controllers, data acquisition, etc.) are

mounted in a 19" frame in the upper part of the rack. The lower part of the rack contains a hydrogen peroxide monitor [18] and the TRISTAR and HypHOP pump. The whole rack as mounted inside HALO is shown in Fig. 1.

2.1 Optical and mechanical set-up

The optical and mechanical set-up consists of an optical board with a 66 cm × 52 cm footprint, a 2-l liquid nitrogen cryostat (ILK, Dresden) housing three quantum cascade lasers (Alpes Lasers, Lausanne, Switzerland) for CO (2158.30 cm⁻¹), HCHO (1759.72 cm⁻¹) and CH₄ (1298.98 cm⁻¹) operating at constant temperatures between 95 and 135 K and two cryogenic (~78 K) photovoltaic mercury-cadmium-telluride detectors (Kolmar Technologies Inc., Newburyport, USA), a double-corner cube multi-pass cell following the design of White [19] and a set of reflecting optics for beam collimation and stirring. Time multiplexing of the three laser beams is achieved via pneumatically driven pop-up mirrors. Details of the optical set-up are documented in [13, 14, 17].

Both the optical alignment and the laser operation conditions are sensitive to changes in the surrounding temperature and to a lesser extent to changes in the cabin

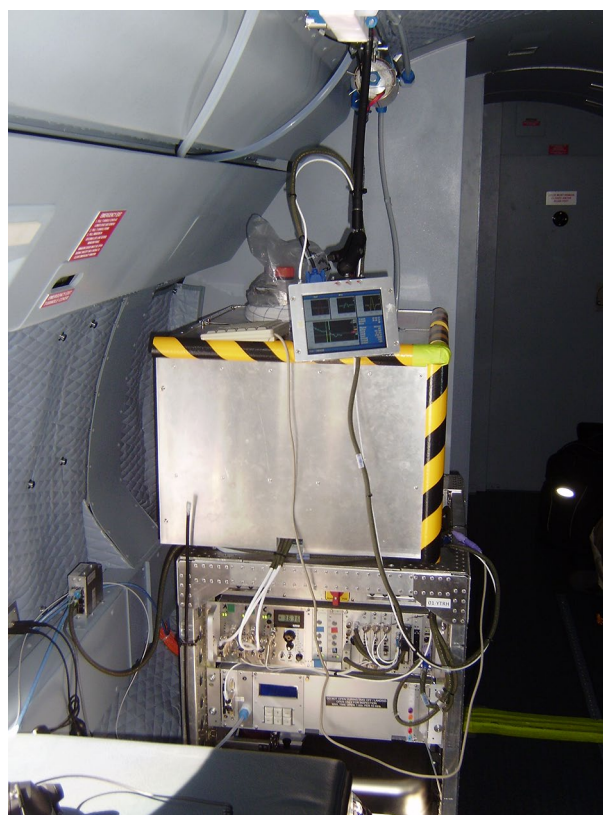


Fig. 1 TRIHOP mounted on board of the HALO aircraft

pressure. Therefore, the optical board and the laser cryostat are enclosed in an aluminum frame with 3 cm of insulation foam (melanin foam) mounted on the inside. Additionally heating foils are glued to the underside of the optical board. The combination of the controlled heating of the optical board and cooling due to boiling-off from the liquid nitrogen cryostat allows the temperature inside the enclosure to be regulated to $(35 \pm 0.1)^\circ\text{C}$, even at cabin temperatures up to 40°C . These measures guarantee a constant temperature of the optics independent of cabin temperature. The time required from start-up of the instrument until stabilization of the instrument temperature is of the order of 2 h. Unfortunately, the aircraft safety instructions require a power shut-off during roll-out and refueling of the plane, resulting in an approximately 30-min interruption of the active temperature stabilization during the final phase before take-off. Although the enclosure is still able to keep the temperature of the optics close to its set-point, the first part of a measurement flight is still affected by slight changes in the optical temperature.

The main effect of pressure variations inside the cabin (at higher altitudes the cabin pressure is reduced to approximately 840 hPa) is the change in boiling temperature of the liquid nitrogen. This can in principle lead to changes in the temperature settings of the lasers and detectors with subsequent changes of the operation conditions. Although the optical board is mounted onto the rack with shock-mounts, accelerations of the aircraft due to ascent, descent or changing of the heading (curves) can potentially induce alignment changes. Additional changes of the cabin pressure can lead to changes in the optical alignment in particular that of the White cell.

2.2 Signal processing and data acquisition

The electronic set-up has been described in detail by Schiller et al. [14]. Briefly, saw-tooth current ramps of 66 ms duration are applied to each laser, sweeping the emission frequency across the target absorption lines. Additionally a 20-kHz sinusoidal component is added to the laser current for wavelength modulation. The amplified detector output from a signal and a reference channel (for active line-locking) undergoes phase-sensitive detection at 40 kHz (2f) with analog lock-in amplifiers (Femto Messtechnik, model LIA-BV-150-S, Berlin, Germany). The data acquisition is very flexible and can be adjusted to the measurement tasks. Since HCHO mixing ratios in the troposphere are 3 orders of magnitude smaller than for CO, the majority of the sampling time is dedicated to this species. Three different measurement modes are distinguished: in-flight calibration (CO, CH₄), background (HCHO) and ambient (CO, CH₄, HCHO) measurements. During calibrations a standard is supplied to the instrument from a tank (6 l composite tank, Auer GmbH, Germany) to

acquire a reference spectrum of known concentration. Ambient spectra are fitted to these calibration spectra. In-flight calibrations for CO and CH₄ are performed every 30 min for 1 min. In-flight calibrations for HCHO are presently not performed. Instead, pre- and post-flight calibrations are performed using a permeation source. In general HCHO measurements are more affected by optical fringes that induce background structures to the spectrum, which are larger than the gas absorption itself. Therefore, regular in-flight background measurements are performed with cabin air after passing a scrubber (platinum pellets heated to 80°C) removing HCHO completely every 144 s for a duration of 35 s. These background spectra are subtracted from ambient HCHO measurements. In-between background measurements ambient measurements are performed in cycles, each consisting of HCHO (5 s), CO (1 s) and CH₄ (1 s). A complete cycle lasts 12 s (including delays due to mirror adjustments) and an ambient measurement period consists of 7 cycles (105 s).

2.3 Inlet configuration

Figure 2 shows the gas flow plan. Ambient air is sampled from an unheated forward facing stainless steel inlet (envi-scope GmbH, Frankfurt, Germany) equipped with a 1/2" PFA liner. Inside the cabin a 1/2" PFA bypass is established with the outlet towards the rear of the aircraft. From this high flow bypass (~few hundred SLM (standard liter per minute)) sample flows to the HypHOP and TRISTAR instruments are drawn by 1/4" PFA tubes. The sample flow for the TRISTAR instrument is 3.3 SLM, yielding a gas exchange time in the White cell (volume 2.7 l) of ~2.5 s at a cell pressure of 50 hPa. Via a Teflon valve either zero air consisting of scrubbed cabin air (heated platinum pellets) or the flow from a gas tank (CO and CH₄ standard) can be used to replace the ambient air flow. During the first test flight described in the following section the gas flow was modified, to sample either gas from the standard directly (calibration mode) or scrubbed standard air (HCHO background).

3 Results from the test flight

On January 24, 2015 a first HALO test flight was performed from Oberpfaffenhofen in Southern Germany as part of the OMO-EU campaign. The purpose of this flight was to test individual instruments installed in the HALO cabin under different flight conditions, with varying ascend and descend rates. During this flight, TRISTAR sampled either standard air from a tank (CO) or scrubbed zero air from the tank (HCHO). Here we will discuss only the results for CO. For ideal conditions one would expect a constant CO signal during all phases of the flight. Any observed changes in the signal

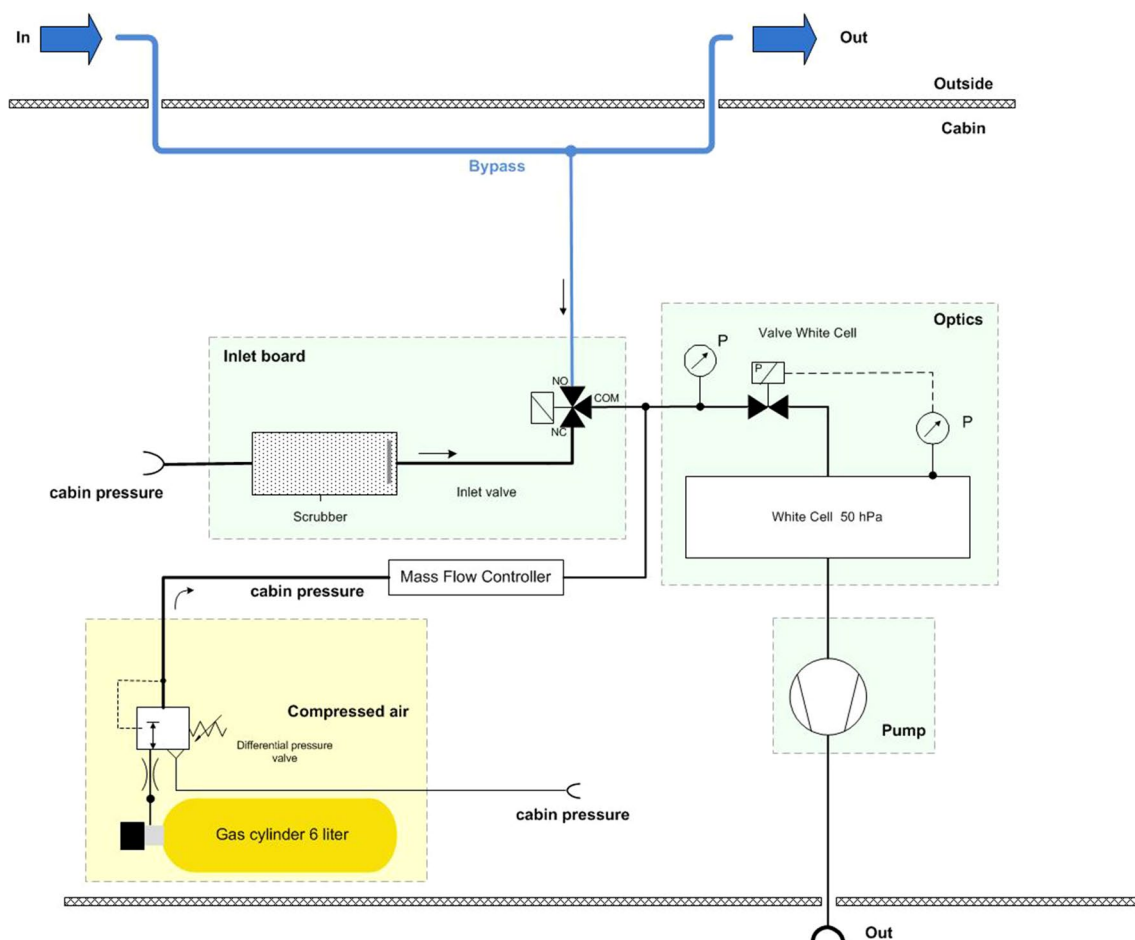


Fig. 2 Sketch of the gas flow plan

are, therefore, due to changes in the instrument stability. Figure 3 shows a time series of the CO mixing ratio signal, altitude, cabin pressure, detector DC level, cabin temperature and the temperature of the optical plate. As mentioned above TRISTAR was operated in a two-laser configuration (HCHO, CO), alternating between the two channels measuring CO for 2 s and HCHO for 7 s. A measurement cycle consists of calibrations for CO (1 min duration) performed every 23 min, background measurements for HCHO by scrubbing tank air for 15 min and “ambient” measurements (7 min tank air) for both CO and HCHO. Note that we will not analyze CO measurements during background, since the scrubbing efficiency of the device used for HCHO was neither constant nor did it remove CO completely. Here we will only use the regular CO calibrations and the “ambient” CO data, both obtained from the tank.

On this particular day, the aircraft was moved out of the hanger around 9:00 in the morning (local time). Before roll-out the instruments were under power for about 2 h in the hanger. During roll-out the power supply

for all experiments was interrupted for about 30 min, with repowering around 9:30. As shown in Fig. 3c the plate temperature decreased from the set value of 31.5 to 8 °C during the power interruption. After restart of the instrument the optical plate is slowly heated up and finally reached the setting point after approx. 2 h. A faster heating would result in a strong swing of the temperature above the setting point, further delaying the temperature stabilization. The CO data for calibrations (green in Fig. 3a) and “ambient” (red) are calculated by fitting to an average master spectrum obtained on the ground around 9:40 (black). The measured “ambient” CO data varied between 241 and 266 ppb_v relative to the master spectrum (mean: 257.1 ppb_v; 1σ standard deviation: 4.91 ppb_v), exhibiting a long-term drift towards higher values and sometimes a sinusoidal drift within individual “ambient” data packages. The long-term drift closely follows the changes in cabin and plate temperature. Although the change in cabin pressure that varies between 950 hPa at low flight levels and 840 hPa at the highest flight level affects the DC signal of the MCT detector, it has no

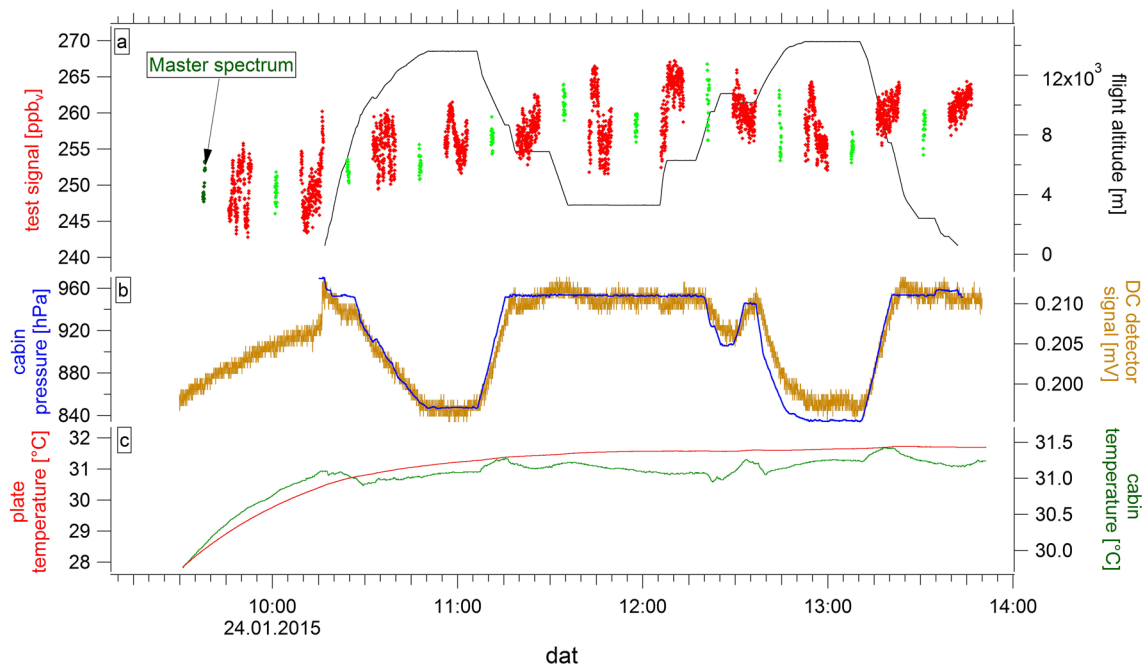


Fig. 3 Results from the HALO test flight on January 24, 2015. Time series for CO and altitude (a), Cabin pressure and DC detector signal (b) and temperatures the cabin and the optical plate (c) are shown

significant influence on the “ambient” data. Obviously, changes in pressure will mainly affect the boiling temperature of the liquid nitrogen used for cooling and thus the operating temperature of the MCT detectors which is not actively stabilized, while the temperature setting of the laser is not affected due to its active temperature control.

To de-trend the “ambient” CO data two different approaches were made. First, we used the standard evaluation protocol for data de-trending that applies linear interpolations between the in-flight calibrations (bright green trace in Fig. 3). The results are shown in Fig. 4 (green trace), which indicates a strong reduction in the overall variability and an elimination of the long-term trend relative to the raw data (red). This leads to reductions in both the mean value (250.93 ppbv) and the 1σ standard deviation (3.11 ppbv). Short-term variations within each “ambient” package cannot be reduced by this measure. Instead of using linear interpolations between succeeding in-flight calibrations we also used a fit of the “ambient” data to the measured plate temperature ($\text{CO} = 2.38 T^2 - 140.08 T + 2313.3$) (blue trace in Fig. 4). This leads to slightly smaller values for the mean (250.1 ppbv) and the standard deviation (2.91 ppbv). Please note the standard deviation is ultimately limited by the variability within “ambient” blocks, which often exhibits almost sinusoidal variations (e.g. around 11:50) corresponding to a mixing ratio of 2.9 ppbv and an optical density of 0.001. These variations, whose magnitude varies strongly over the flight, are

not significantly related to any changes in environmental or instrumental parameters.

To investigate the nature of the variations we will inspect individual absorption spectra during a period with rather small variations (around 13:15, Fig. 5) and a period with strong variation (around 11:50, Fig. 6). Shown in Fig. 5a is a CO spectrum as a function of the channel number (0–255). The spectrum was measured at 13:19 local time. Based on the signal strength (difference between the minimum and maximum between in the fitting range between channel numbers 50–205) and the noise determined from the peak to peak variability outside of the fitting range (channel numbers 0–50 and 205–255), a signal-to-noise ratio (SNR) of 274.13 was determined. A second spectrum in this block was obtained at 13:16 (Fig. 5b) with a SNR of 259.36. Calculating the difference between these two spectra (Fig. 5c) yields a residual with high- and low-frequency etalon structures. These etalon structures strongly increase in amplitude during periods of enhanced variability (e.g. around 11:50). As an example Fig. 6 shows two spectra obtained at 11:42 (Fig. 6a) and 11:44 (Fig. 6b). Stronger etalon structures are already visible in the individual spectra resulting in lower SNRs of 116.81 and 89.49, respectively. The residual (Fig. 6c) clearly shows the increase in the amplitude of the low-frequency etalon structure by roughly a factor of 2 relative to the situation described in Fig. 5c. This is a general behavior as shown in Fig. 7. Strong variability

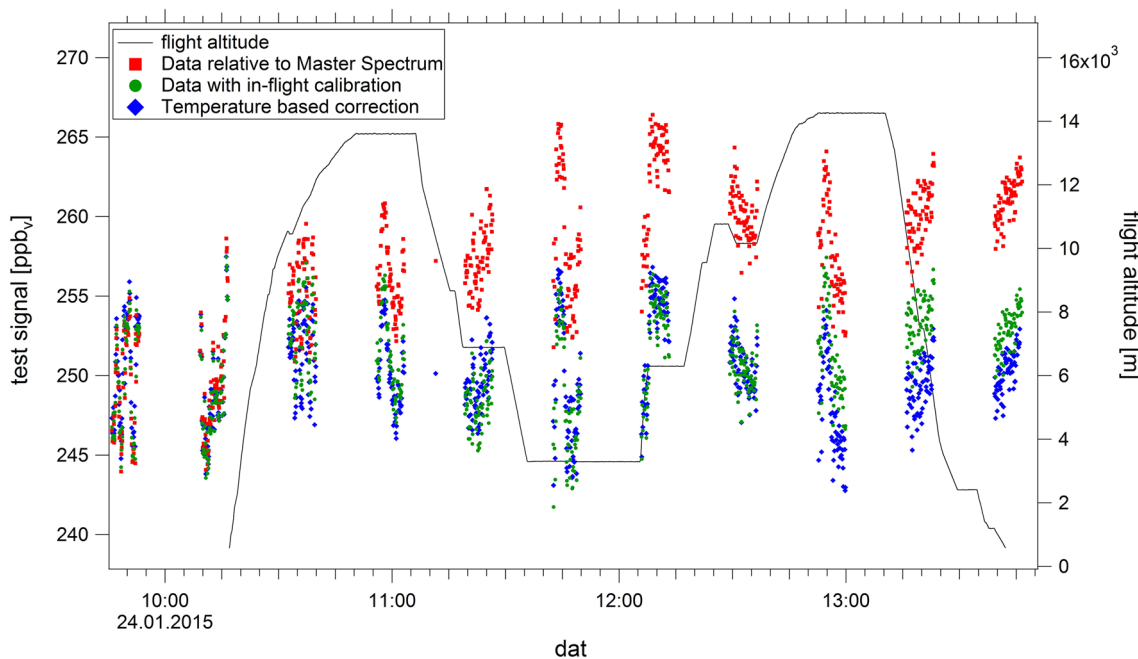


Fig. 4 De-trending of the raw data (*red*) by linear interpolation between in-flight calibrations (*green*) and a polynomial fit to the temperature of the optical plate (*blue*)

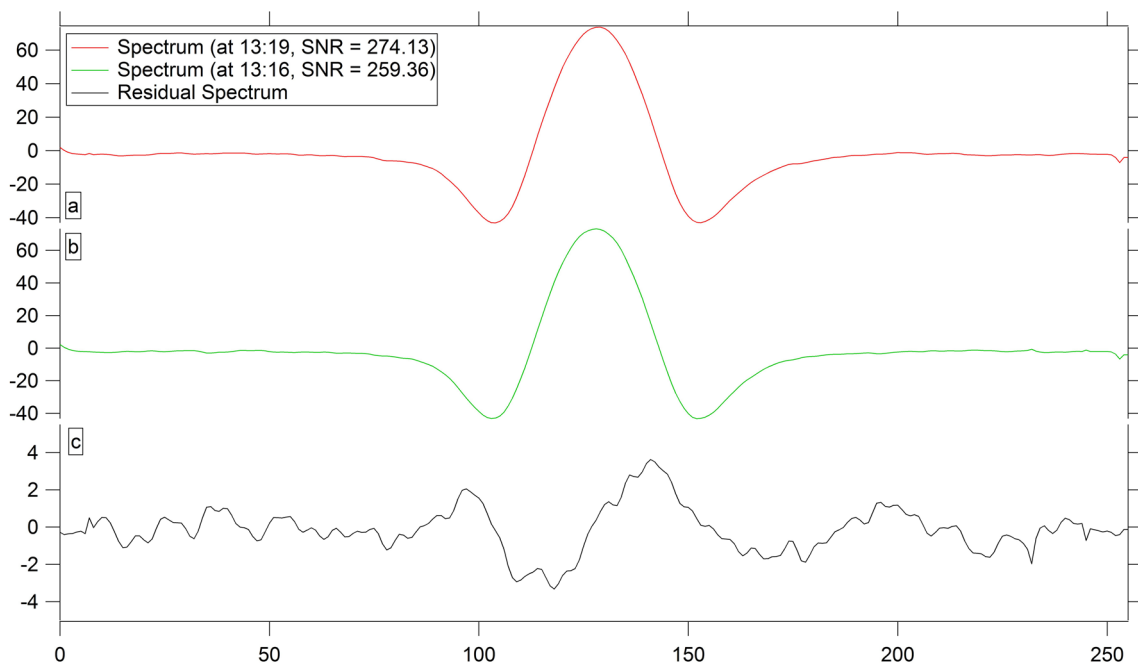


Fig. 5 CC spectra during a period with low variability in CO (**a**, **b**) and the residual after calculating the difference between both spectra (**c**)

within one block of “ambient” CO (Fig. 7a) is associated with low signal-to-noise ratios (Fig. 7b), indicating changes in the phase or amplitude of a superimposed etalon structure. During periods with low CO variability, the etalon structure is generally smaller and more stable,

resulting in increased SNRs. Visual inspections of Fig. 7c indicated that periods with low SNR ratios are often observed after fast ascends or descends of the aircraft documented by the aircraft’s angle of attack (green trace in Fig. 7) and the rate of altitude change (black trace).

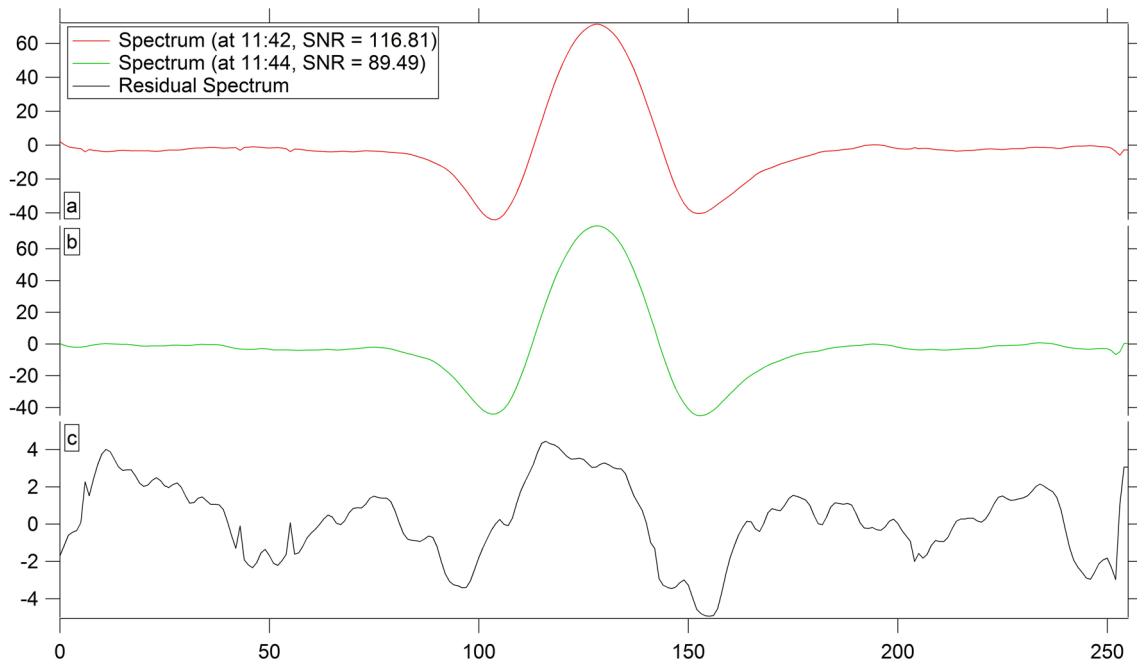


Fig. 6 Same as Fig. 5 for a period with high CO variability and small SNR

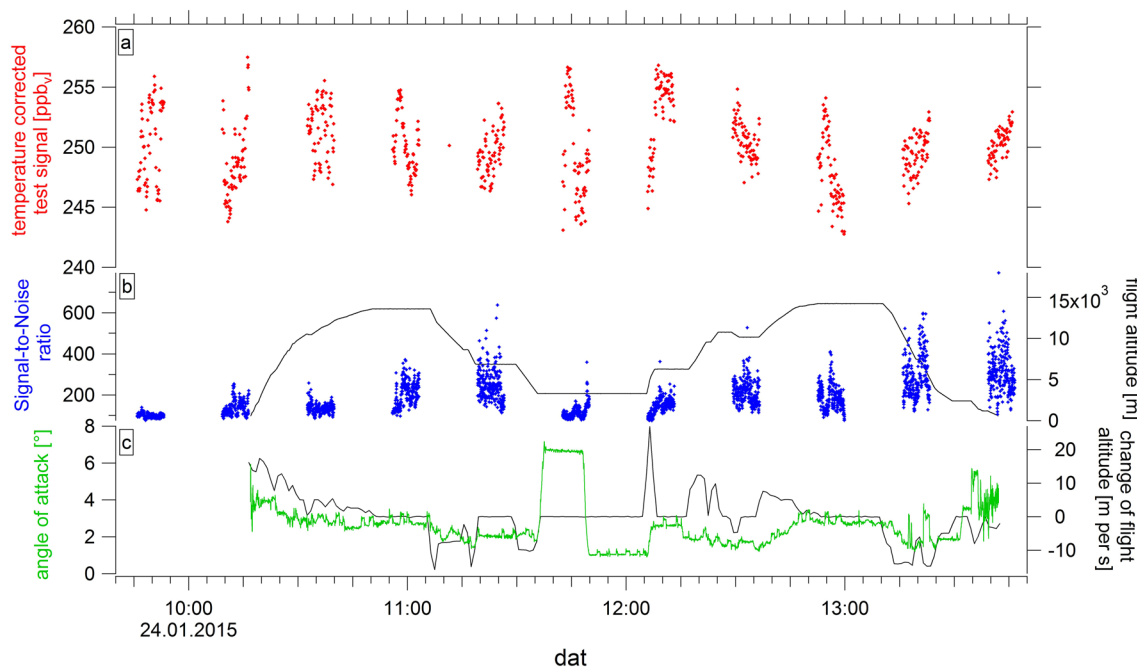


Fig. 7 Drift corrected CO data (a), the signal-to-noise ratio of individual spectra, altitude (b), the aircraft’s angle of attack and the rate of change in altitude during the test flight (c)

This analysis demonstrates that the quality of the CO data is ultimately limited by spectral background structures (fringes) at an optical density level of 0.001. While long-term drifts can be addressed by in-flight calibrations or a de-trending based on a relationship with the temperature

of the optical table, the variability of the short-term fluctuations cannot be removed by these measures. To reduce the etalon effect one could use background subtraction, similar to those performed for HCHO. Unfortunately, the scrubber used for HCHO does not remove CO completely.

The scrubbing efficiency for CO was determined to be $0.84 \pm 0.01\%$ and showed a slight dependency on the temperature of the scrubber and the aircraft's angle of attack. So in order to use CO background measurements, the scrubbing efficiency for CO has to be increased to 100%. It is not clear if this can be achieved with the present design of the scrubber. An alternative method to reduce the influence of the optical fringes on the precision of the CO measurements is the application of wavelet transformation to the CO spectra. As demonstrated by Li et al. [20] for ground-based CO data this can reduce the noise level due to fringes by roughly a factor of 2. In the next chapter we will demonstrate that the actual precision of the CO data in its present form is sufficient for atmospheric studies during OMO-EU.

4 Results from two measurements flights

Two additional measurement flights were performed during OMO-EU on January 25 and January 27, 2015. During both flights ambient CO data were obtained in the troposphere and the lower stratosphere up to a maximum altitude of 14 km. Instead of showing the time series for those flights, we will use the CO data in a correlation plot with O₃ (Fig. 8) measured by the FAIRO instrument, which consists of a chemiluminescence sensor plus an UV photometer [21], achieving a precision better than 1.5% of the reading. O₃-CO correlations can be used to study

trace gas exchange across the tropopause, in particular the mixing of tropospheric and stratospheric air masses across the local tropopause [22, 23]. The method relies on the compact relationship that both trace gases form in the stratosphere and troposphere, respectively. While the O₃ mixing ratio increases strongly in the lower stratosphere, CO exhibits very small mixing ratios (less than 50 ppb_v) above the tropopause. In the troposphere the roles of both species are reversed, with high mixing ratios of CO (more than 100 ppb_v) and low mixing ratios of O₃ in the absence of photochemical production from pollution. In an O₃-CO scatter plot the stratospheric reservoir forms a vertical branch parallel to the O₃ axis, while the tropospheric reservoir forms a horizontal branch parallel to the CO axis. Mixing between these two reservoirs across the local tropopause can be deduced from mixing lines that connect these two branches. Since the stratospheric branch of the correlation is characterized by low variability in CO mixing ratios, high precision is required for its identification. As shown in Fig. 8, as expected the CO variability at potential temperatures above the tropopause (dark red data points) strongly decreases with increasing O₃ levels. At the highest O₃ mixing ratio (~1200 ppb_v) the 3 σ -variability for CO (which is a combination of both ambient variability and the measurement precision) is of the order of 10 ppb_v, slightly larger than the 3 σ measurement precision deduced from the test flight, indicating that the CO measurement precision is sufficient for atmospheric measurements.

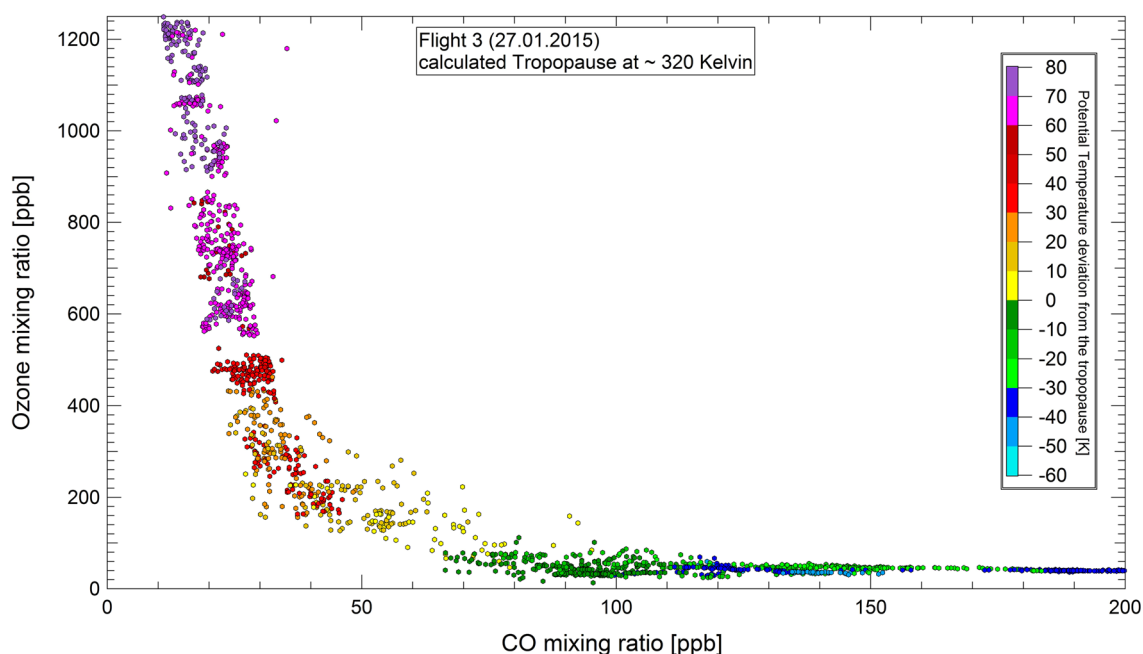


Fig. 8 O₃-CO correlation during the measurement flight on January 27, 2015. See text for details

5 Conclusions

Here we used a test flight on the HALO aircraft during the OMO-EU mission to identify noise sources and stability limitations for CO measurements obtained from mid-IR laser absorption spectroscopy. During the flight, the instrument was probed with a constant mixing ratio from an on-board gas tank, normally used for in-flight CO and CH₄ calibrations. Ideally this should produce a constant signal during all phases of the flight. Deviations, in particular a long-term drift, are due to slow changes in the temperature of the optical plate during the first 2 h of a measurement flight. Although the temperature of the optics is actively stabilized, an unavoidable power break during the roll-out of the aircraft out of the hangar is responsible for the temperature drift of the optics and subsequently the drift in measured CO data. Regular in-flight calibrations or a temperature-CO mixing ratio polynomial relation can be used to successfully de-trend the data. Ultimately, the precision is limited to values around 3 ppb_v by changes in the amplitude or phase of optical fringes similar to those limiting the detection limit for HCHO [14]. To overcome this problem, regular high-frequency background measurements for CO would be required. Such background measurements are already performed for HCHO, but the scrubber used has an insufficient scrubbing efficiency for CO, which is of the order of 85% (100% for HCHO), requiring a redesign. An alternative solution to suppress the influence of the optical fringes could be the application of a wavelet transformation to individual absorption spectra, as has been demonstrated for ground-based CO measurements [20]. Nevertheless, an analysis of ambient data obtained during two measurement flights demonstrates that the CO data quality is sufficient for atmospheric studies.

Acknowledgements Open access funding provided by Max Planck Society. This research was part of the OMO-EU campaign. Thanks to Andreas Zahn and his colleagues from Karlsruhe Institute of Technology for providing the ozone data. Also we would like to thank Torsten Schmitt for his contribution to the post-processing of the data sets. Last but not least, we want to thank the whole OMO community for realizing the campaign.

Open Access This article is distributed under the terms of the Creative Commons Attribution 4.0 International License (<http://creativecommons.org/licenses/by/4.0/>), which permits unrestricted use, distribution, and reproduction in any medium, provided you give appropriate credit to the original author(s) and the source, provide a link to the Creative Commons license, and indicate if changes were made.

References

1. H.I. Schiff, G.I. Mackkay, J. Bechera, *Air monitoring by spectroscopic techniques* (Wiley, Chichester, 1994)
2. D.J. Brassington, *Advances in spectroscopy*, vol. 24 (Wiley, Chichester, 1994)
3. P. Werle, *Spectrochim. Acta A* **52**, 805 (1996)
4. M. Tacke, F. Wiebhold, R. Grisar, H. Fischer, F.-J. Lübken, *Encyclopedia of analytical chemistry* (Wiley, Chichester, 2000)
5. C.R. Webster, G.J. Flesch, D.S. Scott, J.E. Swanson, R.D. May, W.S. Woodward, C. Gmachl, F. Capasso, D.L. Sivco, J.N. Bailargeon, A.L. Hutchinson, A.Y. Cho, *Appl. Opt.* **40**, 321 (2001)
6. R. Kormann, R. Königstedt, U. Parchatka, J. Lelieveld, H. Fischer, *Rev. Sci. Instrum.* **76**, 075102 (2005)
7. J.S. Li, W. Chen, H. Fischer, *Appl. Spectrosc. Rev.* **48**, 523 (2013)
8. G.L. Sachse, G.F. Hill, L.O. Wade, M.G. Perry, *J. Geophys. Res.* **92**(D2), 2071 (1987)
9. H.I. Schiff, D.R. Karecki, G.W. Harris, D.R. Hastie, G.I. Mackay, *J. Geophys. Res.* **95**(D7), 10147 (1990)
10. C.R. Webster, R.D. May, C.A. Trimble, R.A. Chave, J. Kendall, *Appl. Opt.* **33**, 454 (1994)
11. M. Loewenstein, H. Jost, J. Grose, J. Eilers, D. Lynch, S. Jensen, J. Marmie, *Spectrochim. Acta A* **58**, 2329 (2002)
12. A. Fried, P. Weibring, D. Richter, J. Walega, *Proc. SPIE* **7222**, 7222202–7222221 (2009)
13. F.G. Wienhold, H. Fischer, P. Hoor, V. Wagner, R. Königstedt, G.W. Harris, J. Andres, R. Grisar, M. Knothe, W.J. Riedel, F.-J. Lübken, T. Schilling, *Appl. Phys. B* **67**, 411 (1998)
14. C.L. Schiller, H. Bozem, C. Gurk, U. Parchatka, R. Königstedt, G.W. Harris, J. Lelieveld, H. Fischer, *Appl. Phys. B* **92**, 419 (2008)
15. G.W. Santoni, B.C. Daube, E.A. Kort, R. Jimenez, S. Park, J.V. Pittman, E. Gottlieb, B. Xiang, M.S. Zahniser, D.D. Nelson, J.B. McManus, J. Peischl, T.B. Ryerson, J.S. Holloway, A.E. Andrews, C. Sweeney, B. Hall, E.J. Hints, F.L. Moore, J.W. Elkins, D.F. Hurst, B.B. Stephens, J. Bent, S.C. Wofsy, *Atmos. Meas. Technol.* **7**, 1509–1526 (2014)
16. S. Müller, P. Hoor, F. Berkes, H. Bozem, M. Klingebiel, P. Reutter, H.G.J. Smit, M. Wendisch, P. Spichtinger, S. Borrmann, *Geophys. Res. Lett.* **42**, 949–955 (2015)
17. R. Kormann, H. Fischer, C. Gurk, F. Helleis, Th Klüpfel, K. Kowalski, R. Königstedt, U. Parchatka, V. Wagner, *Spectrochim. Acta A* **58**, 2489 (2002)
18. T. Klippel, H. Fischer, H. Bozem, M.G. Lawrence, T. Butler, P. Jöckel, H. Tost, M. Martinez, H. Harder, E. Regelin, R. Sander, C.L. Schiller, A. Stickler, J. Lelieveld, *Atmos. Chem. Phys.* **11**, 4391 (2011)
19. J.U. White, *J. Opt. Soc. Am.* **66**, 411 (1976)
20. J. Li, B. Yu, H. Fischer, *Appl. Spectrosc.* **69**, 496 (2015)
21. A. Zahn, J. Weppner, H. Widmann, K. Schlote-Holubek, B. Burger, T. Kühner, H. Franke, *Atmos. Meas. Technol.* **5**, 363 (2012)
22. H. Fischer, F.G. Wienhold, P. Hoor, O. Bujok, C. Schiller, P. Siegmund, M. Ambaum, H.A. Scheeren, J. Lelieveld, *Geophys. Res. Lett.* **27**, 97 (2000)
23. P. Hoor, C. Gurk, D. Brunner, M.I. Hegglin, H. Wernli, H. Fischer, *Atmos. Chem. Phys.* **4**, 1427 (2004)